# CHAPTER IV
# COMPARISON OF SINGLE-WALLED CARBON NANOTUBES PRODUCED BY USING DIFFERENT CATALYSTS*

## 4.1 Abstract

A series of monometallic and bimetallic catalysts on various oxide supports has been tested for the production of single-walled carbon nanotubes (SWNTs) by either disproportionation of CO or decomposition of $CH_4$ at 750 °C. The catalysts were prepared by incipient wetness impregnation using transition metal solutions among Co, Ni, Fe, and Mo on three different oxide supports which are $SiO_2$, MgO, and $Al_2O_3$. In this study, the effects of transition metals, metal ratios in a bimetallic catalyst, oxide catalyst supports, and carbon-containing gases on both quality and quantity of SWNTs were investigated. In order to compare the as-prepared SWNTs obtained from a variety of spent catalysts, temperature programmed oxidation (TPO) and Raman spectroscopy were used to evaluate total carbon yield, and selectivity towards SWNTs. In addition, transmission electron microscope (TEM) was utilized to confirm the nanostructure of resulting carbonaceous products. Among the tested catalysts in this study, the disproportionation reaction of CO over silica supported Co-Mo catalysts showed the best SWNTs quality based on data obtained from TPO and Raman spectroscopy.

## 4.2 Introduction

Since Ijima has discovered carbon nanotubes in soot in 1993 [1] Carbon nanotubes have captured attention of researcher worldwide due to their exceptional physical and chemical properties that can be extended to a great number of potential applications [2].

Single-wall carbon nanotubes (SWNTs) can be considered as the building blocks for nano-size material. It can be produced by arc discharge [1,3,4], pulsed laser vaporization [5,6,7], and catalytic decomposition of carbon-containing gas [8-28]. The first two methods are operated by vaporizing graphite target at extremely

* To be submitted to the Journal of Solid State Communications

high temperature (>3000°C). Therefore, it is difficult to expand the production scale to commercial level. Among them, heterogeneous catalytic decomposition is a promising technique for large-scale production at a relatively low cost. Hence, the investigation of catalyst formulations and operating conditions is widely interested.

For heterogeneous catalytic decomposition technique, SWNTs can be produced by disproportionation of CO over supported catalysts such as $Mo/Al_2O_3$ [8,9], $Co\text{-}Mo/SiO_2$ (CoMoCAT) [10] and $Fe\text{-}Mo/Al_2O_3$ [9,11], or over metal nanoparticles such as $Fe(CO)_5$ (HiPCO) [12] and $Ni(CO)_4$ [13]. Moreover, decomposition of $CH_4$ was reported to be an alternative carbon source for SWNTs production by using $Fe/SiO_2$ [14], Co/MgO [15,16], Fe/MgO [15,17], Ni/MgO [15], $Co\text{-}Mo/MgO$ [18], $Co\text{-}Fe/MgO$ [15], $Fe/Al_2O_3$ [14,19,20], and $Fe\text{-}Mo/Al_2O_3$ [21-23]. While the operating conditons for all investigation are ranging from 500 to 1200°C and 1 to 10 atm. In addition to disproportionation of CO and decomposition of $CH_4$, catalytic vapor deposition of hydrocarbons such as ethylene [9,24], acetylene [25,26], benzene [27], and toluene [28] has also been reported.

This study focuses on the production of SWNTs by comparing the catalyst formulations and carbon-containing gas. Also, a number of parameters, obtained from characterization results of the spent catalysts, are defined and used to find the active catalysts for SWNTs production, which can also be used in further development of the catalyst.

## 4.3 Experimental Section

### 4.3.1 Materials

#### *4.3.1.1 Metal Precursors and Catalyst Supports*

Iron(III) nitrate nonahydrate ($Fe(NO_3)_3.9H_2O$ with a purity above 98%, cobalt(II) nitrate hexahydrate ($Co(NO_3)_2.6H_2O$) with a purity above 98%, Nickel(II) nitrate hexahydrate ($Ni(NO_3)_2.6H_2O$) in crystalline form, and ammonium molybdate(VI) tetrahydrate ($(NH_4)_6Mo_7O_{24}.4H_2O$) with 81.0-83.0% as $MoO_3$ were used as catalyst precursors. Three different catalyst supports used in this

study are as following: Silica gel ($SiO_2$) having particle sizes in the range of 70-230 mesh (62-210 μm) with an average pore diameter of 6 nm, a BET surface area of 480 $m^2/g$, and a pore volume of 0.75 $cm^3/g$. Magnesium oxide (MgO) is a fused type and has a particle size of -40 mesh (minus 40 mesh refers to material that has been sized by passing through a screen with 40 holes per inch) with a BET surface area of 4.1 $m^2/g$. γ-Alumina (γ-$Al_2O_3$) is a weakly acidic type and has an average particle size of 150 mesh (104 μm), pore size of 5.8 nm, and a BET surface area of 155 $m^2/g$. All the metal precursors and catalyst supports were supplied by Sigma-Aldrich Co. Ltd. and were used as received without any further purification.

#### *4.3.1.2 Gases*

Air zero was used in the catalyst calcination. Hydrogen, with a purity of 99.99%, was used for the pre-reduction of the catalyst in the SWNT synthesis step. Helium, with a purity of 99.99%, was used as an inert gas in the heating step of the SWNT synthesis. 2% oxygen in helium balance was used as an oxidizing agent in the temperature-programmed oxidation (TPO) experiment. All of the above gases were supplied by Thai Industrial Gas Co. Ltd. Carbon monoxide gas, with a purity of 95%, was obtained from Airgas Inc. Methane, with a purity of 99.99%, was supplied by Thai Industrial Gas Co. Ltd.

### 4.3.2 Methodology

#### *4.3.2.1 Catalyst Preparation*

A series of supported catalysts including monometallic catalysts (Fe, Co, and Ni) and bimetallic catalysts (Fe-Mo, Co-Mo, and Ni-Mo) was prepared by incipient wetness impregnation technique on the oxide supports ($SiO_2$, MgO, and $Al_2O_3$). For all catalyst formulations, a total metal loading on the support was kept constant at 6 wt%. In case of bimetallic catalysts, three different molar ratios (2:1, 1:1, and 1:2) were prepared to investigate the synergism from each metal couple. After impregnation, the catalyst samples were first dried in air at room temperature

for 2 h, then dried overnight in oven at 120°C, and finally calcined in the flow of dry-air at 500°C for 3 h.

*4.3.2.2 Synthesis of Carbon Nanotubes*

The calcined catalyst (0.5 g) was placed in a 0.5-in horizontal quartz tubular reactor, heated in a $H_2$ flow to 500°C (100 $cm^3$/min), held on this temperature for 30 min, and then heated in a flow of He to 750°C (100 $cm^3$/min). Subsequently, CO or $CH_4$ was introduced at a flow rate of 100 $cm^3$/min at 1 atm and the reactor was kept under these conditions for 30 min. At the end of the reaction, the system was cooled down to room temperature under the flow of He.

*4.3.2.3 Temperature-Programmed Oxidation (TPO)*

The total amount of deposited carbon on the spent catalyst was obtained by TPO following the method described elsewhere [17]. A total peak area obtained from TPO profile of each sample is related to the combustible fraction in the spent catalyst. The total carbon yield is defined as the weight of the combustible fraction as a percentage of the weight of spent catalyst, as shown in the following equation:

$$\text{Carbon yield}(\%) = \frac{\text{Weight of combustible fraction}}{\text{Weight of spent catalyst}} \times 100$$

Selectivity of the different forms of deposited carbon was evaluated by fitting the TPO profiles into separated peaks of gaussian-lorentzian mixtures by using PeakFit software. It must be noted that the peaks centered around 500-530°C represent the carbon in the form of SWNTs [29]. The peaks centered at a lower temperature represent the carbon in the form of disordered carbon, where the peaks centered at a higher temperature represent the carbon in the form of MWNTs and other graphitic carbons. However, the shape and position of a TPO peak may be varied with the catalyst composition and with the kinetics of the oxidation process and the amount of carbon on the surface. From the fitting of the TPO profiles, the error in the peak positions was less than ±20°C. The areas under the splitted peaks

have been used to calculate the selectivity of disordered carbon, SWNTs, and MWNTs in the spent catalyst and to calculate the TPO quantity parameter, as shown by the following equations:

$$\text{Selectivity (\%)} = \frac{\text{Area under the peaks in the region of specified carbon structure}}{\text{Total peak area}} \times 100$$

$$\text{TPO quantity parameter} = \frac{\text{Area under the peaks in the region of SWNTs and MWNTs}}{\text{Total peak area}} \times 100$$

*4.3.2.4 Raman Spectroscopy*

Raman spectroscopy was performed in a Jovin Yvon-Horiba Lab Ram equipped with a charge-coupled detector and with He-Ne laser (632 nm) as excitation source. Raman spectra were obtained by using 3.0-5.0 mW laser power; 15s integration time for each spectrum; and ten Raman spectra were averaged for each sample. From the Raman spectra, the presence of SWNTs in the sample can be directly obtained from the appearance of radial breathing mode (RBM) which occurs below 300 $cm^{-1}$ [30]. Raman signals in the RBM range can also be used to estimate tube diameter of SWNTs. The presence of graphite-like structures, i.e. SWNTs, MWNTs, graphite nanostructure, etc., can be obtained from the appearance of the in-plane stretching mode of ordered crystalline graphite-like structures (G band) that is ranging from 1,400 to 1,700 $cm^{-1}$. Moreover, the indication on the level of disordered carbon can be obtained from the analysis on the D band which occurs at around 1,350 $cm^{-1}$. The Raman spectra were fitted by using gaussian-lorentzian mixtures in the PeakFit software to obtain the peak areas in D band and G band. The error in the peak positions was less than ±5 $cm^{-1}$. From the areas of D band and G band, the Raman quality parameter is defined as the following equation:

$$\text{Raman quality parameter} = \frac{G}{D+G} \times 100$$

Where D represents the peak area in the D band, and G represents the peak area in the G band.

*4.3.2.5 Transmission Electron Microscopy (TEM)*

Transmission electron microscopy was performed on a JEOL JEM-2000FX at an acceleration voltage of 200 kV. The sample was prepared by sonicating the spent catalyst in an isopropanol solutions, putting a few drops of the suspension onto a lacey carbon grid, and then allowing it to dry.

## 4.4 Results and Discussion

### 4.4.1 Characterization of Deposited Carbon by TPO and Raman Spectroscopy

Figure 4.1 shows an example of normalized TPO profiles of the spent Co-Mo 1:2/$SiO_2$ catalysts after decomposition of pure CO or $CH_4$. Obviously, the total peak area of $CH_4$ sample is much larger than that of CO sample, indicating higher amount of deposited carbon. The calculated carbon yields of CO and $CH_4$ samples were 1.8 and 15.7 wt%, respectively. After the profiles were fitted, the CO sample was found to contain 10% amorphous carbon, 75% SWNTs, and 15% MWNTs. In case of the $CH_4$ sample, the selectivity of amorphous carbon of 4%, SWNTs of 24%, and MWNTs of 72% was obtained. Moreover, the selectivity of all carbonaceous products was then used to evaluate the TPO quantity parameters, which are 90 for CO sample and 96 for $CH_4$ sample.

Figure 4.2 shows an example of Raman spectra of the spent Co-Mo 1:2/$SiO_2$ catalysts after decomposition of CO and $CH_4$. It is clearly seen that, in case of $CH_4$ sample, no signal in the radial breathing mode (RBM) region was observed, therefore this sample did not contain SWNTs. On the contrary, the Raman spectra of CO sample showed the presence of SWNTs because there are signals in RBM region. In addition to the analysis on the RBM region, the size of D band and G band has also been used as qualitative measurement on the formation of undesirable forms of carbon at which we called this parameter as Raman quality parameter. From the fitted results, the Raman quality parameters of CO and $CH_4$ samples are 95 and 38, respectively.

From the analysis on the TPO and Raman results it can be said that, even though the $CH_4$ sample shows the selectivity towards SWNTs, but there is no

evidence of RBM from the Raman result. Since the fitting of the TPO peak came from a mathematical solution, therefore, the quantitative analysis of TPO results should be used together with the qualitative analysis of Raman results.

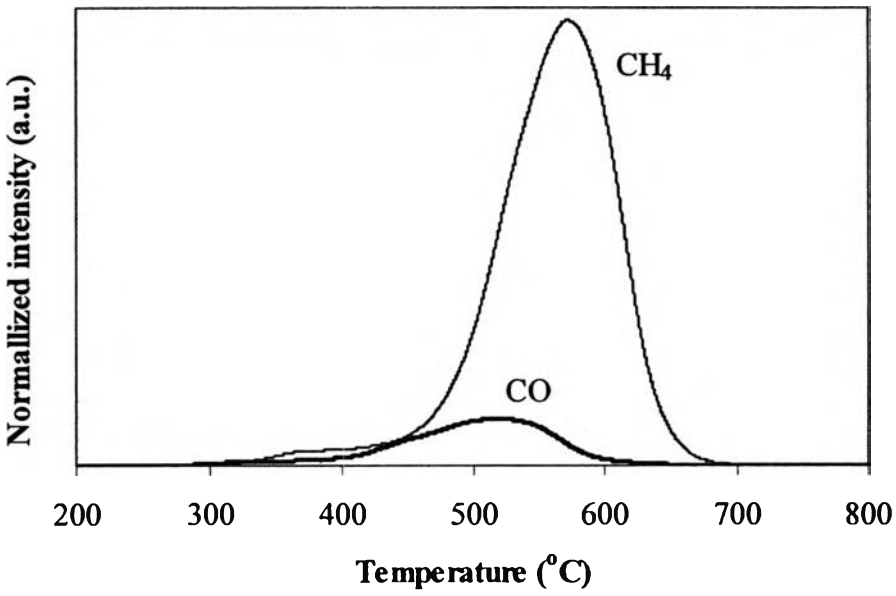


**Figure 4.1** Normalized TPO profiles of spent Co-Mo 1:2/$SiO_2$ catalysts after decomposition of CO and $CH_4$.

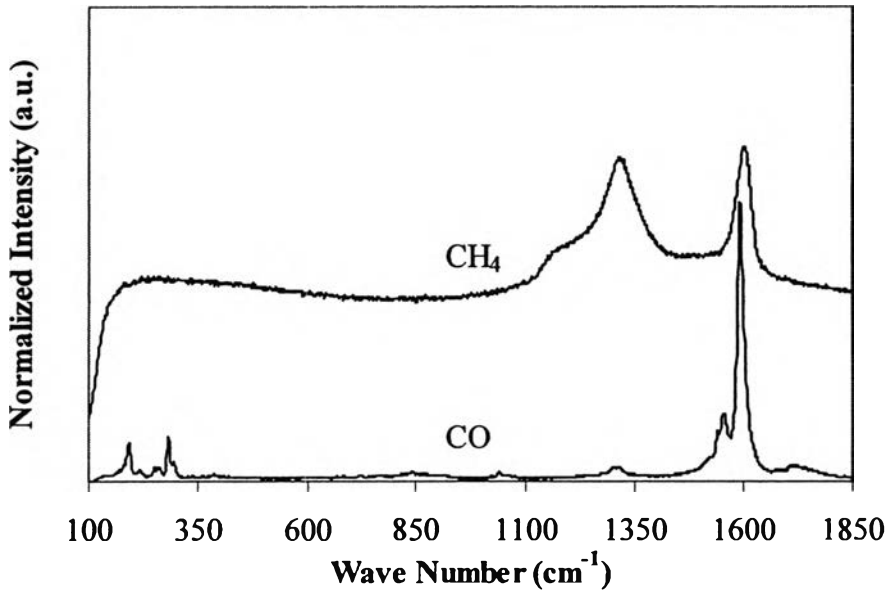


**Figure 4.2** Raman spectra of spent Co-Mo 1:2/$SiO_2$ catalysts after decomposition of different gases at 750°C.

### 4.4.2 Comparison of the Deposited Carbons on $SiO_2$-Supported Catalysts

Characterizations of the spent catalysts by Raman spectroscopy and TPO provides the information of both quality and quantity of the deposited carbons and the results were represented by using histograms and lines. As illustrated in Figure 4.3, the hollow bars represent the percentage of total carbon yield on the left axis, while on the right axis, the lines with circles show the selectivity towards SWNTs and the lines with stars indicate the TPO quantity parameter. The Raman quality parameters are also represented as the lines with diamonds. The samples having the RBM signals were indicated by solid diamonds, while the samples with no RBM signal were indicated by hollow diamonds.

Figure 4.3a and Table 4.1 show the characterization results of the spent $SiO_2$-supported catalysts after the disproportionation of CO. A low carbon yield in a range of 0.3-2.3 wt% was obtained from all catalysts, while the carbon yield from bimetallic catalysts is higher than that from monometallic catalysts. Regardless of $Fe/SiO_2$ and $Mo/SiO_2$, a degree of carbon nanotubes for all catalysts, as indicated by the Raman quality parameter and TPO quantity parameter, is higher than 50. In this series, the bimetallic catalysts exhibit better performance of producing the carbon nanotubes than monometallic catalyst, because of the higher observed parameters. Moreover, all bimetallic samples demonstrate the presence of SWNTs in RBM region of Raman spectra, where it cannot be observed on all monometallic samples. A maximum selectivity towards SWNTs as high as 75 and a maximum of both quality and quantity parameter as high as 95 and 90, respectively, was obtained from a Co-Mo $1{:}2/SiO_2$ catalyst. Therefore, the Co-Mo $1{:}2/SiO_2$ catalyst is considered the best $SiO_2$-supported catalyst for the production of SWNTs by disproportionation of CO. TEM images of the as-prepared product from Co-Mo $1{:}2/SiO_2$ and Ni-Mo $2{:}1/SiO_2$ catalysts after disproportionation of CO are shown in Figures 4.4 and 4.5, respectively. From both figure, it is obvious that the product consists primarily of bundles of SWNTs. Small metallic particles of less than 5 nm were found as impurity in the Co-Mo 1:2 sample , while the large metal particles which are not responsible for the growth of SWNTs was found in the Ni-Mo 2:1 sample.

The characterization results of the spent $SiO_2$-supported catalysts after the decomposition of $CH_4$ are shown in Figure 4.3b and Table 4.2. The total carbon yield on the bimetallic samples is greatly improved to a range of 6.2-16.2 wt% from that on the monometallic samples, which contained the carbon content less than 1.0 wt%. However, none of the RBM signals was observed on any spent $SiO_2$-supported catalysts after the decomposition of $CH_4$. The TPO quantity parameter and the selectivity indicate that most of the deposited carbon on the bimetallic samples is in the form of carbon nanotubes, especially MWNTs, where the disordered carbon is a major product from the monometallic catalysts. In this series of catalysts, the carbon nanotubes can be produced by using Fe-Mo 1:2/$SiO_2$ or Co-Mo1:2/$SiO_2$ catalyst.

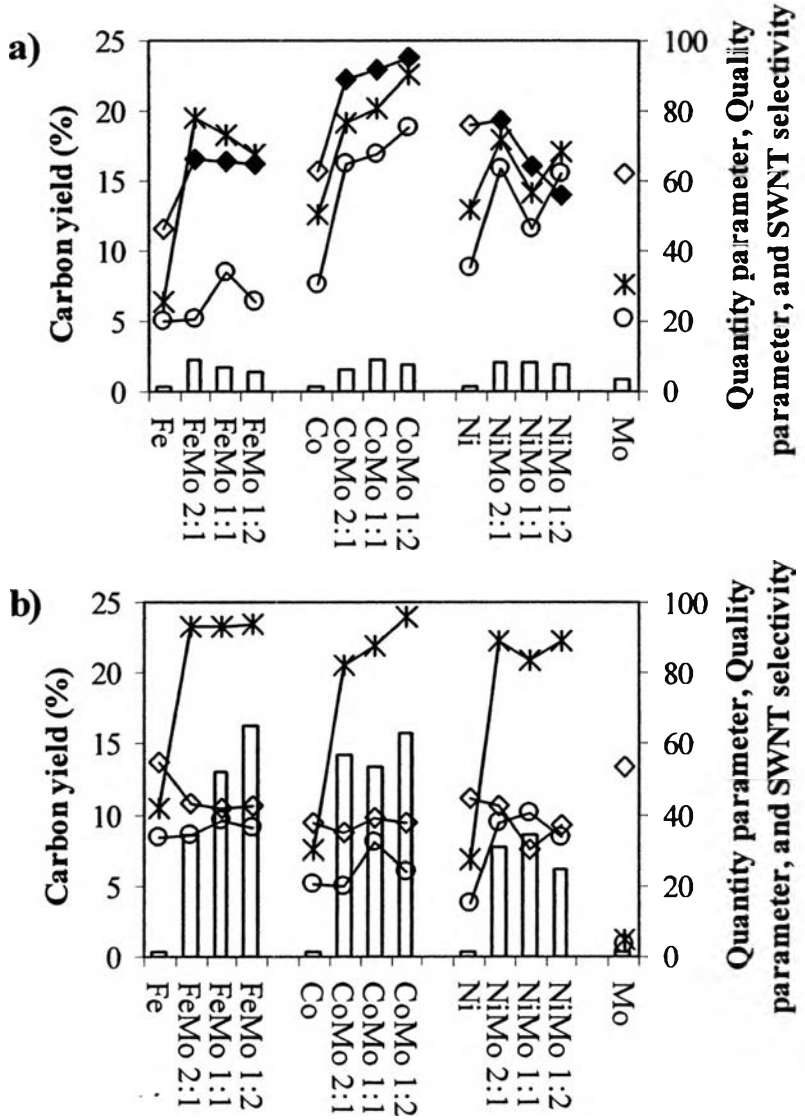


**Figure 4.3** Carbon yield (bar), selectivity towards SWNTs (circle), TPO quantity parameter (star), Raman quality parameter (diamond), and the presence of SWNTs (solid diamond = RBM active, hollow diamond = no RBM signal) of spent $SiO_2$-supported catalysts after (a) the disproportionation of CO and (b) the decomposition of $CH_4$.

**Table 4.1** Selectivity, total carbon yield, TPO quantity parameter, Raman quality parameter, and the presence of RBM signal of spent $SiO_2$-supported catalysts after the disproportionation of CO

| Gas and Catalysts | Selectivity towards carbon structures (%) | | | Total carbon yield (%) | TPO quantity parameter | Raman quality parameter | RBM signal |
|---|---|---|---|---|---|---|---|
| CO, $SiO_2$ | Disordered carbon | SWNTs | MWNTs | | | | |
| Fe | 74 | 20 | 5 | 0.3 | 26 | 47 | No |
| FeMo 2:1 | 22 | 20 | 58 | 2.3 | 78 | 66 | Yes |
| FeMo 1:1 | 27 | 34 | 39 | 1.8 | 73 | 66 | Yes |
| FeMo 1:2 | 33 | 25 | 42 | 1.4 | 67 | 65 | Yes |
| Co | 50 | 31 | 20 | 0.4 | 50 | 63 | No |
| CoMo 2:1 | 23 | 65 | 12 | 1.5 | 77 | 89 | Yes |
| CoMo 1:1 | 19 | 68 | 13 | 2.3 | 81 | 92 | Yes |
| CoMo 1:2 | 10 | 75 | 15 | 1.8 | 90 | 95 | Yes |
| Ni | 48 | 35 | 17 | 0.3 | 52 | 76 | No |
| NiMo 2:1 | 28 | 63 | 9 | 2.0 | 72 | 77 | Yes |
| NiMo 1:1 | 44 | 46 | 10 | 2.1 | 56 | 64 | Yes |
| NiMo 1:2 | 32 | 62 | 6 | 1.9 | 68 | 56 | Yes |
| Mo | 69 | 21 | 10 | 0.9 | 31 | 62 | No |

**Table 4.2** Selectivity, total carbon yield, TPO quantity parameter, Raman quality parameter, and the presence of RBM signal of spent $SiO_2$-supported catalysts after the decomposition of $CH_4$

| Gas and Catalysts | Selectivity towards carbon structures (%) | | | Total carbon yield (%) | TPO quantity parameter | Raman quality parameter | RBM signal |
|---|---|---|---|---|---|---|---|
| **$CH_4$, $SiO_2$** | Disordered carbon | SWNTs | MWNTs | | | | |
| Fe | 58 | 34 | 8 | 0.3 | 42 | 55 | No |
| FeMo 2:1 | 7 | 34 | 59 | 8.6 | 93 | 43 | No |
| FeMo 1:1 | 7 | 38 | 55 | 13.0 | 93 | 42 | No |
| FeMo 1:2 | 6 | 36 | 58 | 16.2 | 94 | 43 | No |
| Co | 70 | 21 | 10 | 0.3 | 30 | 38 | No |
| CoMo 2:1 | 18 | 20 | 62 | 14.2 | 82 | 35 | No |
| CoMo 1:1 | 13 | 32 | 55 | 13.3 | 87 | 39 | No |
| CoMo 1:2 | 4 | 24 | 72 | 15.7 | 96 | 38 | No |
| Ni | 73 | 15 | 13 | 0.3 | 27 | 45 | No |
| NiMo 2:1 | 11 | 38 | 51 | 7.7 | 89 | 42 | No |
| NiMo 1:1 | 16 | 41 | 43 | 8.5 | 84 | 30 | No |
| NiMo 1:2 | 11 | 34 | 55 | 6.2 | 89 | 37 | No |
| Mo | 95 | 3 | 2 | 0.4 | 5 | 53 | No |

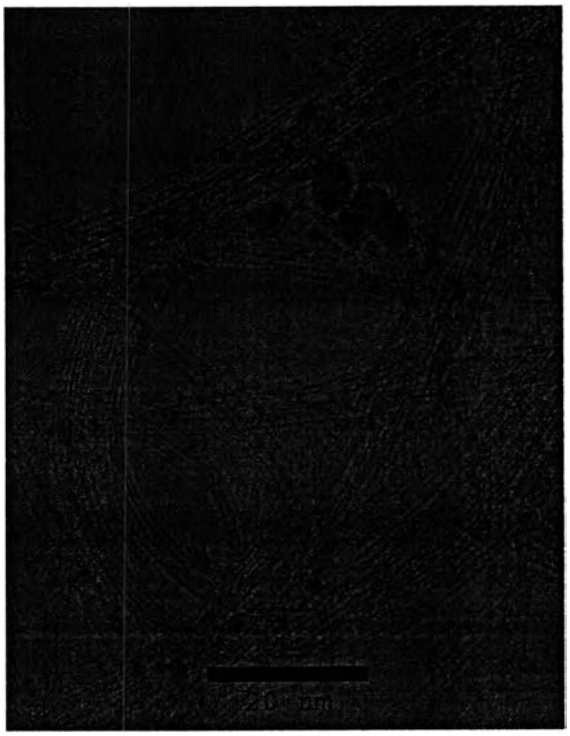

**Figure 4.4** TEM image of spent Co-Mo 1:2/$SiO_2$ after disproportionation of CO at 750°C.

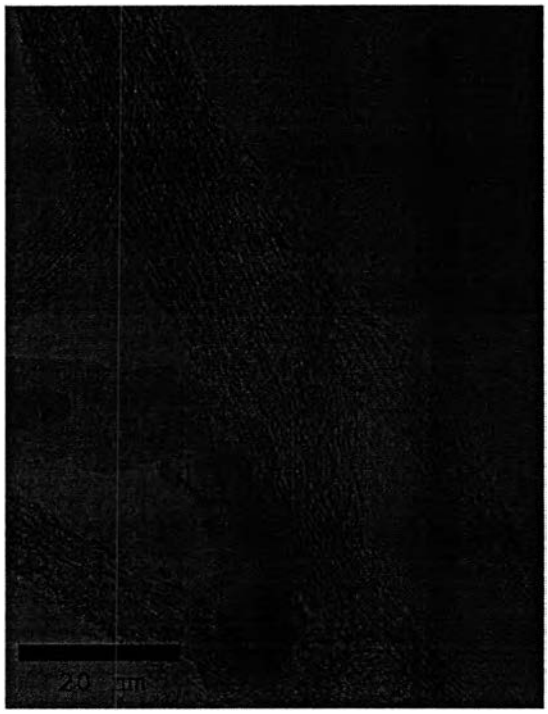

**Figure 4.5** TEM image of spent Ni-Mo 2:1/$SiO_2$ after disproportionation of CO at 750°C.

4.4.3 Comparison of the Deposited Carbons on MgO-Supported Catalysts

Figure 4.6a and Table 4.3 illustrate the characterization results of the spent MgO-supported catalysts after the disproportionation of CO. No more than 1 wt% of carbon yield was obtained from all monometallic catalysts, while a higher carbon yield in the range of 5.5-14.7 wt% was obtained from bimetallic catalysts. The selectivity towards SWNTs from this series was found in the range of 3-24%, where only the Co/MgO sample exhibits the RBM signal. From the quantity parameter and the selectivity, most of the deposited carbons on bimetallic catalysts are in the form of MWNTs. The selectivity towards MWNTs from Fe-Mo and Co-Mo catalysts was found to be highest among the catalysts tested in this study. It is interesting to note that, the tendency of Raman quality parameter on each type of metal are contrary to that of TPO quantity parameter, this may be due to the fluorescence effect caused by the scattered light on the sample.

The characterization results of the spent MgO-supported catalysts after the decomposition of $CH_4$ are exhibited in Figure 4.6b and Table 4.4. All spent monometallic catalysts have the carbon content less than 1 wt%, while the spent bimetallic catalysts have the carbon content at the range of 8.4-23.3 wt%. The spent Fe-Mo 1:1 and Ni-Mo 1:1 catalysts are the only two samples, among all tested catalysts, that contain the deposited carbon higher than 20 wt%. The selectivity towards SWNTs was found in a range of 14-31%, while the RBM signals exist only on the Fe, Fe-Mo 2:1, Co, Co-Mo 2:1, and Ni samples. From the TPO quantity parameter and the selectivity, a major product from monometallic catalysts is disordered carbon and that from bimetallic catalysts is MWNTs. However, in this series of catalysts, the tendency of Raman quality parameter on each type of metal are also contrary to that of TPO quantity parameter. A TEM image of SWNTs from Co/MgO-supported catalysts after decomposition of $CH_4$ is shown in Figure 4.7. This image confirm the values of TPO quantity parameter that a number of SWNTs in the form of bundles was found together with small amount of MWNTs and a large extent of disordered carbon and metallic particle.

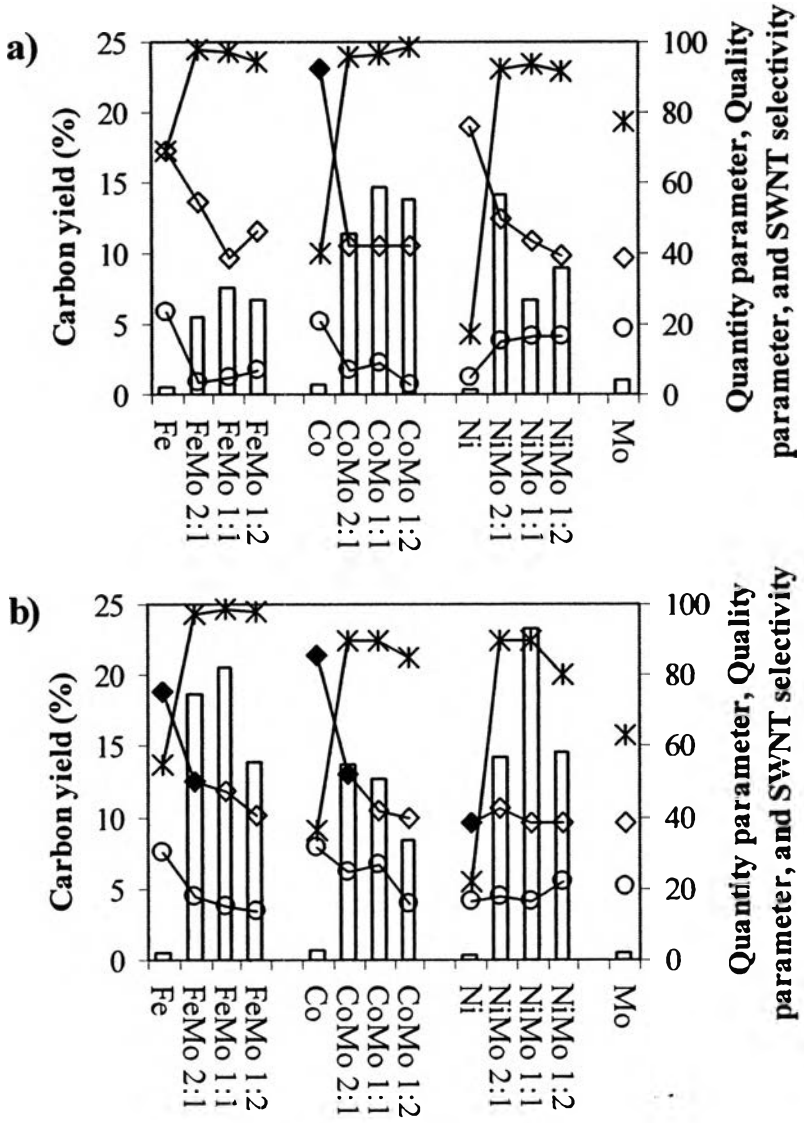


**Figure 4.6** Carbon yield (bar), selectivity towards SWNTs (circle), TPO quantity parameter (star), Raman quality parameter (diamond), and the presence of SWNTs (solid diamond = RBM active, hollow diamond = no RBM signal) of spent MgO-supported catalysts after (a) the disproportionation of CO and (b) the decomposition of $CH_4$.

**Table 4.3** Selectivity, total carbon yield, TPO quantity parameter, Raman quality parameter, and the presence of RBM signal of spent MgO-supported catalysts after the disproportionation of CO

| Gas and Catalysts | Selectivity towards carbon structures (%) | | | Total carbon yield (%) | TPO quantity parameter | Raman quality parameter | RBM signal |
|---|---|---|---|---|---|---|---|
| **CO, MgO** | Disordered carbon | SWNTs | MWNTs | | | | |
| Fe | 31 | 24 | 45 | 0.6 | 69 | 69 | No |
| FeMo 2:1 | 2 | 3 | 94 | 5.5 | 98 | 54 | No |
| FeMo 1:1 | 3 | 5 | 92 | 7.6 | 97 | 39 | No |
| FeMo 1:2 | 6 | 7 | 87 | 6.7 | 94 | 46 | No |
| Co | 60 | 20 | 19 | 0.8 | 40 | 93 | Yes |
| CoMo 2:1 | 4 | 7 | 89 | 11.4 | 96 | 42 | No |
| CoMo 1:1 | 3 | 9 | 88 | 14.7 | 97 | 42 | No |
| CoMo 1:2 | 2 | 3 | 95 | 13.8 | 98 | 42 | No |
| Ni | 83 | 5 | 13 | 0.3 | 17 | 76 | No |
| NiMo 2:1 | 7 | 15 | 77 | 14.2 | 93 | 50 | No |
| NiMo 1:1 | 6 | 17 | 77 | 6.8 | 94 | 43 | No |
| NiMo 1:2 | 8 | 16 | 75 | 9.0 | 92 | 39 | No |
| Mo | 22 | 18 | 59 | 1.0 | 78 | 39 | No |

**Table 4.4** Selectivity, total carbon yield, TPO quantity parameter, Raman quality parameter, and the presence of RBM signal of spent MgO-supported catalysts after the decomposition of $CH_4$

| Gas and Catalysts | Selectivity towards carbon structures (%) | | | Total carbon yield (%) | TPO quantity parameter | Raman quality parameter | RBM signal |
|---|---|---|---|---|---|---|---|
| **$CH_4$, MgO** | Disordered carbon | SWNTs | MWNTs | | | | |
| Fe | 45 | 30 | 24 | 0.6 | 55 | 75 | Yes |
| FeMo 2:1 | 3 | 18 | 80 | 18.6 | 97 | 50 | Yes |
| FeMo 1:1 | 2 | 15 | 83 | 20.5 | 98 | 47 | No |
| FeMo 1:2 | 2 | 14 | 84 | 13.8 | 98 | 41 | No |
| Co | 64 | 31 | 5 | 0.6 | 36 | 85 | Yes |
| CoMo 2:1 | 11 | 25 | 65 | 13.8 | 89 | 52 | Yes |
| CoMo 1:1 | 10 | 27 | 63 | 12.6 | 90 | 42 | No |
| CoMo 1:2 | 15 | 16 | 70 | 8.4 | 85 | 40 | No |
| Ni | 78 | 17 | 5 | 0.4 | 22 | 39 | Yes |
| NiMo 2:1 | 11 | 18 | 72 | 14.2 | 89 | 42 | No |
| NiMo 1:1 | 11 | 16 | 73 | 23.3 | 89 | 39 | No |
| NiMo 1:2 | 20 | 22 | 59 | 14.5 | 80 | 38 | No |
| Mo | 37 | 21 | 43 | 0.6 | 63 | 39 | No |

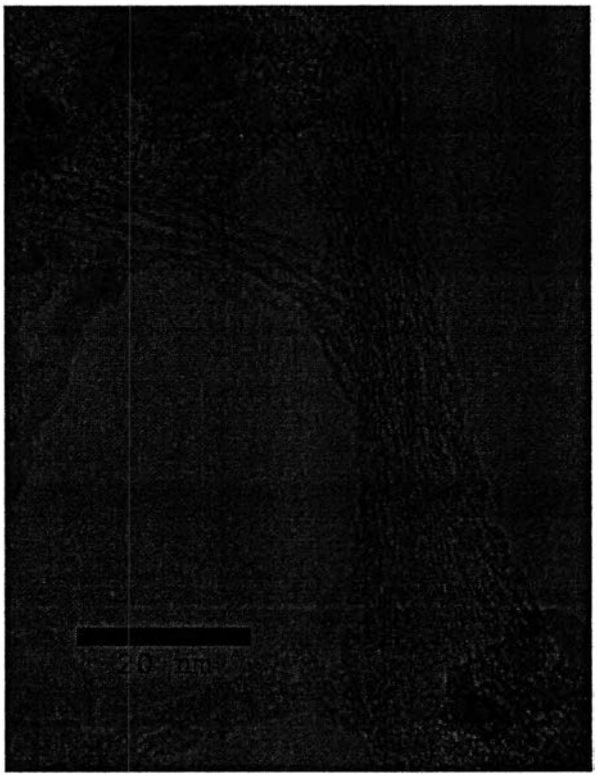


**Figure 4.7** TEM image of spent Co /MgO after decomposotion of $CH_4$ at 750°C.

4.4.4 Comparison of the Deposited Carbons on $Al_2O_3$-Supported Catalysts

Figure 4.8a and Table 4.5 demonstrate the results of the spent $Al_2O_3$-supported catalysts after the disproportionation of CO. A low carbon yield less than 1.0 wt% was obtained from monometallic catalysts. The range of carbon yield from bimetallic $Al_2O_3$-supported catalysts (3.0-5.1 wt%) was found in between that from bimetallic $SiO_2$-supported catalysts and bimetallic MgO-supported catalysts. The selectivity towards SWNTs is in a range of 16-50%, while only bimetallic catalysts provide RBM signals. From the TPO quantity parameter and selectivity, carbon nanotubes above 80% can be obtained from most of the bimetallic catalysts, in which the Co-Mo 2:1 provide a maximum on both carbon yield and carbon nanotubes selectivity. In Figure 4.9, a TEM image of spent Co-Mo $1:1/Al_2O_3$ after disproportionation of CO showed that the carbon product from this catalysts mostly

contained a number of large-sized and individual carbon nanotubes. It also contained large metallic particles and some extent of disordered carbon.

The characterization results of the spent $Al_2O_3$-supported catalysts after the decomposition of $CH_4$ are illustrated in Figure 4.8b and Table 4.6. Total carbon yield in a range 0.3 to 1.1 wt% was obtained from monometallic Fe, Co, and Ni samples, whereas the Mo sample provide a maximum of 8.6 wt% among all spent monometallic catalysts. For the bimetallic catalysts, the carbon yield in a small range of 11.3-14.7 wt% was obtained. The selectivity towards SWNTs was found in a range of 16-61%, where only bimetallic Fe-Mo and Co-Mo samples show the presence of RBM signal. The Raman quality parameter less than 50% was obtained from this series of catalysts, but the tendency is comparable to that of TPO quantity parameter. From the quantity parameter and selectivity, carbon nanotubes more than 80% of selectivity can be produced by all Ni-Mo, Co-Mo 1:1, and Mo catalysts, whereas SWNTs more than 50% of selectivity can be produced by Fe-Mo 1:1 and Fe-Mo 1:2 catalysts.

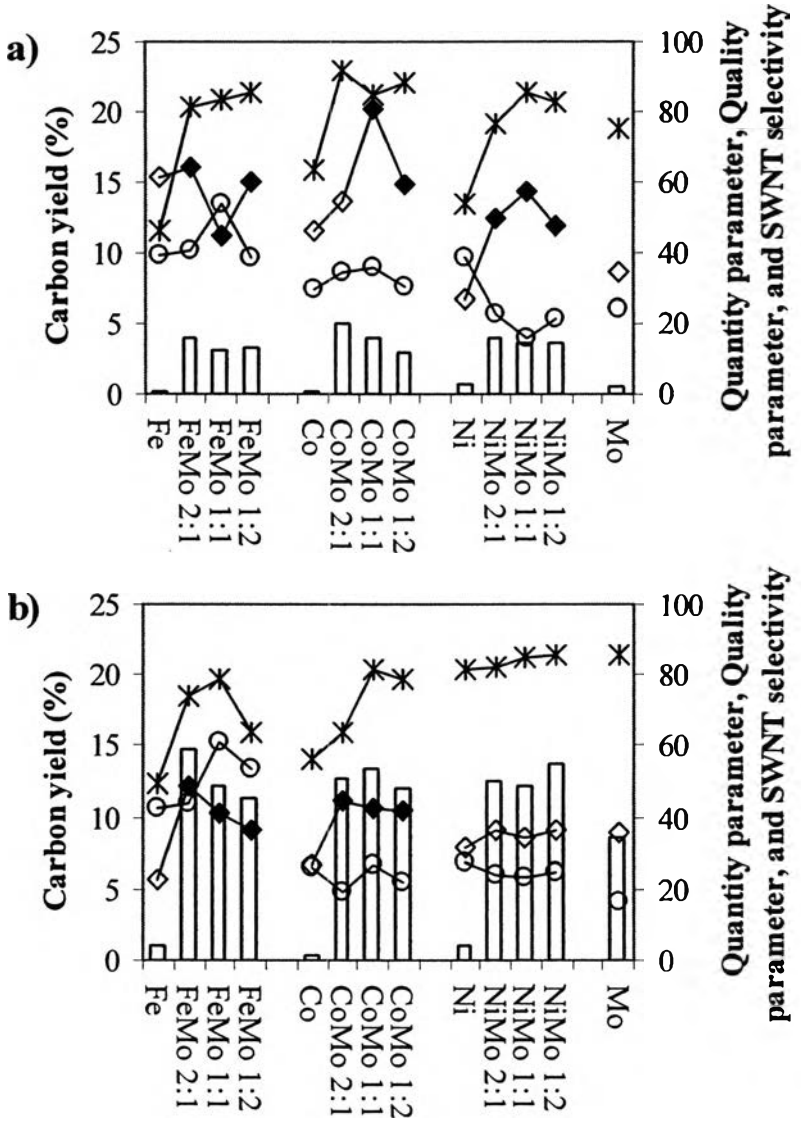


**Figure 4.8** Carbon yield (bar), selectivity towards SWNTs (circle), TPO quantity parameter (star), Raman quality parameter (diamond), and the presence of SWNTs (solid diamond = RBM active, hollow diamond = no RBM signal) of spent $Al_2O_3$-supported catalysts after (a) the disproportionation of CO and (b) the decomposition of $CH_4$.

**Table 4.5** Selectivity, total carbon yield, TPO quantity parameter, Raman quality parameter, and the presence of RBM signal of spent $Al_2O_3$-supported catalysts after the disproportionation of CO

| Gas and Catalysts | Selectivity towards carbon structures (%) | | | Total carbon yield (%) | TPO quantity parameter | Raman quality parameter | RBM signal |
|---|---|---|---|---|---|---|---|
| **CO, $Al_2O_3$** | Disordered carbon | SWNTs | MWNTs | | | | |
| Fe | 54 | 39 | 7 | 0.1 | 46 | 61 | No |
| FeMo 2:1 | 18 | 41 | 41 | 3.9 | 82 | 64 | Yes |
| FeMo 1:1 | 16 | 54 | 30 | 3.2 | 84 | 45 | Yes |
| FeMo 1:2 | 14 | 39 | 47 | 3.3 | 86 | 60 | Yes |
| Co | 37 | 29 | 34 | 0.1 | 63 | 46 | No |
| CoMo 2:1 | 8 | 35 | 57 | 5.1 | 92 | 55 | No |
| CoMo 1:1 | 15 | 36 | 48 | 4.0 | 85 | 80 | Yes |
| CoMo 1:2 | 11 | 30 | 58 | 3.0 | 89 | 60 | Yes |
| Ni | 46 | 39 | 15 | 0.6 | 54 | 27 | No |
| NiMo 2:1 | 23 | 23 | 54 | 3.9 | 77 | 50 | Yes |
| NiMo 1:1 | 14 | 16 | 70 | 3.6 | 86 | 57 | Yes |
| NiMo 1:2 | 17 | 21 | 62 | 3.6 | 83 | 47 | Yes |
| Mo | 25 | 24 | 51 | 0.5 | 75 | 35 | No |

**Table 4.6** Selectivity, total carbon yield, TPO quantity parameter, Raman quality parameter, and the presence of RBM signal of spent $Al_2O_3$-supported catalysts after the decomposition of $CH_4$

| Gas and Catalysts | Selectivity towards carbon structures (%) | | | Total carbon yield (%) | TPO quantity parameter | Raman quality parameter | RBM signal |
|---|---|---|---|---|---|---|---|
| **$CH_4$, $Al_2O_3$** | Disordered carbon | SWNTs | MWNTs | | | | |
| Fe | 51 | 43 | 6 | 1.0 | 49 | 22 | No |
| FeMo 2:1 | 26 | 44 | 30 | 14.7 | 74 | 49 | Yes |
| FeMo 1:1 | 21 | 61 | 18 | 12.1 | 79 | 41 | Yes |
| FeMo 1:2 | 36 | 53 | 11 | 11.3 | 64 | 37 | Yes |
| Co | 44 | 26 | 30 | 0.3 | 56 | 27 | No |
| CoMo 2:1 | 36 | 19 | 45 | 12.7 | 64 | 45 | Yes |
| CoMo 1:1 | 18 | 27 | 55 | 13.3 | 82 | 43 | Yes |
| CoMo 1:2 | 21 | 22 | 56 | 12.1 | 79 | 42 | Yes |
| Ni | 19 | 27 | 54 | 1.1 | 81 | 31 | No |
| NiMo 2:1 | 17 | 24 | 58 | 12.6 | 83 | 36 | No |
| NiMo 1:1 | 15 | 23 | 62 | 12.1 | 85 | 34 | No |
| NiMo 1:2 | 14 | 25 | 61 | 13.7 | 86 | 36 | No |
| Mo | 15 | 16 | 69 | 8.6 | 85 | 35 | No |

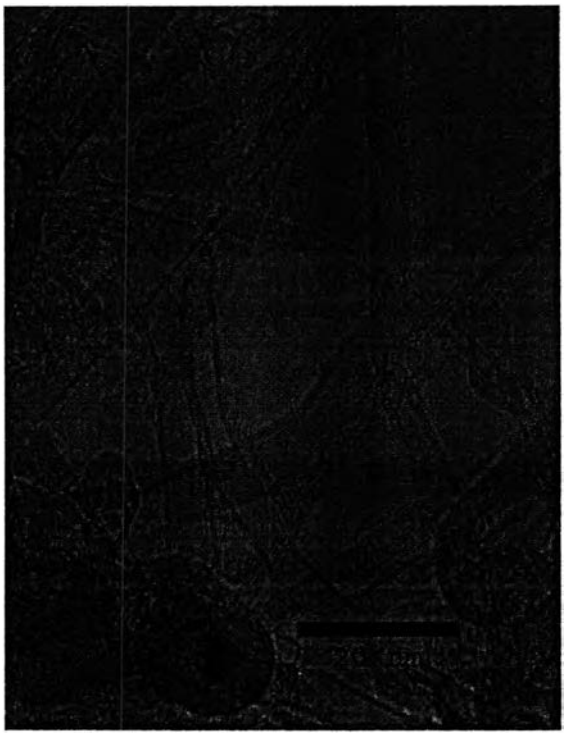

**Figure 4.9** TEM image of spent Co-Mo 1:1/$Al_2O_3$ after disproportionation of CO at 750°C.

## 4.5 Conclusions

In this work, the active catalysts for producing SWNTs by using disproportionation of CO and catalytic decomposition of $CH_4$ over a series of monometallic and bimetallic catalysts supported on various oxide supports have been investigated. Based on the all results obtained from characterization, the catalysts that provide the selectivity towards SWNTs more than 60% are all bimetallic Co-Mo/$SiO_2$ with CO, Ni-Mo 2:1/$SiO_2$ with CO, Ni-Mo 1:2/$SiO_2$ with CO, and Fe-Mo 1:1/$Al_2O_3$ with $CH_4$. The highest selectivity towards SWNTs of 75% was obtained from the Co-Mo 1:2/$SiO_2$ with CO, while the highest total carbon yield of 12.1 wt% was obtained from the Fe-Mo 1:1/$Al_2O_3$ with $CH_4$.

However, the catalysts that were suitable for production of MWNTs and both forms of carbon nanotubes can be obtained in this study. In case of MWNTs

production, more than 85% of MWNT selectivity was obtained from disproportionation of CO on all bimetallic Fe-Mo/MgO and Co-Mo/MgO catalysts. The highest MWNT selectivity of 95% was found on Co-Mo 1:2/MgO sample, while the carbon yield as high as 14.7 wt% was obtained from Co-Mo 1:1/MgO sample. To produced both forms of carbon nanotubes, the highest TPO quantity parameter of 98% was obtained from Fe-Mo 2:1/MgO with CO, Co-Mo 1:2/MgO with CO, Fe-Mo 1:1/MgO with $CH_4$ and Fe-Mo 1:2 with $CH_4$, in which the highest carbon yield of 20.5 wt% was obtained from Fe-Mo 1:1/MgO with $CH_4$ gas.

## 4.6 Acknowledgements

This work cannot be successful without the participation of the following individuals and organizations.

It is a great pleasure to acknowledge the Thailand Research Fund (TRF) for supporting this research work and also for providing a Ph.D. Scholarship under the Royal Golden Jubilee Program to Mr. Pisan Chungchamroenkit.

I would like to give special thanks to Dr. Ummarawadee Yanatatsaneejit for her valuable suggestion and comments. In addition, I would like to thank Dr. Nataphan Sakulchaicharoen for taking transmission electron microscope images.

I would also like to take this opportunity to thank CPO, Poon Arjpru, who helped to set up electrical parts of our experimental set-up.

Finally, special thanks are also offered to all the faculty members and staff of the Petroleum and Petrochemical College and the School of Chemical, Biological, and Materials Engineering at the University of Oklahoma for providing all facilities needed for this research work.

## 4.7 REFERENCES

[1] S. Iijima, T. Ichihashi, Nature 363 (1993) 603.

[2] B.I. Yakobson, R.E. Smalley, Am. Sci. 85 (1997) 324.

[3] D.S. Bethune, C.H. Kiang, M.S. de Vries, G. Gorman, R. Savoy, J. Vasquez, R. Beyers, Nature 363 (1993) 605.

[4] C. Journet, W.K. Maser, P. Bernier, A. Loiseau, M.L. Delachapelle, S. Lefrant, P. Deniard, R. Lee, J.E. Fischer, Nature 388 (1997) 756.

[5] T. Guo, P. Nikolaev, A. Thess, D.T. Colbert, R.E. Smalley, Chem. Phys. Lett. 243 (1995) 49.

[6] W.K. Maser, E. Muoz, A.M. Benito, M.T. Martinez, G.F. de la Fuente, Y. Maniette, E. Anglaret, J.L. Sauvajol, Chem. Phys. Lett. 292 (1998) 587.

[7] A.M. Rao, S. Bandow, E. Richter, P.C. Eklund, Thin Solid Films 331 (1998) 141.

[8]. H. Dai, A.G. Rinzler, P. Nikolaev, A. Thess, D.T. Colbert, R.E. Smalley, Chem. Phys. Lett. 260 (1996) 471.

[9] J.H. Hafner, M.J. Bronikowski, B.R. Azamian, P. Nikolaev, A.G. Rinzler, D.T. Colbert, K.A. Smith, R.E. Smalley, Chem. Phys. Lett. 296 (1998) 195.

[10] B. Kitiyanan, W.E. Alvarez, J.H. Harwell, D.E. Resasco, Chem. Phys. Lett. 317 (2000) 497.

[11] B. Zheng, Y. Li, J. Liu, Appl. Phys. A. 74 (2002) 345.

[12] P. Nikolaev, M.J. Bronikowski, R.K. Bradley, F. Rohmund, D.T. Colbert, K.A. Smith, R.E. Smalley, Chem. Phys. Lett. 313 (1999) 91.

[13] E. Plonjes, P. Palm, G.B. Viswanathan, V.V. Subramaniam, I.V. Adamovich, W.R. Lempert, H.L. Fraser, J.W. Rich, Chem. Phys. Lett. 352 (2002) 342.

[14]. J. Kong, A.M. Cassel, H. Dai, Chem. Phys. Lett. 292 (1998) 567.

[15] J.-F. Colomer, C. Stephan, S. Lefrant, G. Van Tendeloo, I. Willems, Z. Konya, A. Fonseca, Ch. Laurent, J.B. Nagy, Chem. Phys. Lett. 317 (2000) 83.

[16] J.-F. Colomer, J.-M. Benoit, C. Stephan, S. Lefrant, G. Van Tendeloo, J.B. Nagy, Chem. Phys. Lett. 345 (2001) 11.

[17] H. Yan, Q. Li, J. Zhang, Z. Liu, Carbon 40 (2002) 2693.

[18] S. Tang, Z. Zhong, Z. Xiong, L. Sun, L. Liu, J. Lin, Z.X. Shen, K.L. Tan, Chem. Phys. Lett 350 (2001) 19.

[19] A. Peigney, P. Coquay, E. Flahaut, R.E. Vandenberghe, E.D. Grave, Ch. Laurent, J. Phys. Chem. B. 105 (2001) 9699.

[20] Ch. Laurent, A. Peigney, E. Flahaut, A. Rousset, Mat. Res. Bull. 35 (2000) 661.

[21] G.L. Hornyak, L. Grigorian, A.C. Dillon, P.A. Parilla, K.M. Jones, M.J. Heben, J. Phys. Chem. B. 106 (2002) 2821.

[22] B.C. Liu, S.C. Lyu, T.J. Lee, S.K. Choi, S.J. Eum, C.W. Yang, C.Y. Park, C.J. Lee, Chem. Phys. Lett. 373 (2003) 475.

[23] M. Su, B. Zheng, J. Liu, Chem. Phys. Lett. 322 (2000) 321.

[24] S.C. Lyu, B.C. Liu, S.H. Lee, C.Y. Park, H.K. Kang, C.W. Yang, C.J. Lee, J. Phys. Chem. B. 108 (2004) 1613.

[25] B.C. Liu, S.C. Lyu, S.I. Jung, H.K. Kang, C.-W. Yang, J.W. Park, C.Y. Park, C.J. Lee, Chem. Phys. Lett. 383 (2004) 104.

[26] H.J. Jeong, K.H. An, S.C. Lim, M.-S. Park, J.-S. Chang, S.-E. Park, S.J. Eum, C.W. Yang, C.-Y. Park, Y.H. Lee, Chem. Phys. Lett. 380 (2003) 263.

[27]. H.M. Cheng, F. Li, G. Su, H.Y. Pan, L.L. He, X. Sun, M.S. Dresselhaus, Appl. Phys. Lett. 72 (1998) 3282.

[28] H. Ago, S. Ohshima, K. Uchida, M. Yumura, J. Phys. Chem. B. 105 (2001) 10453.

[29] W.E. Alvarez, B. Kitiyanan, A. Borgna, D.E. Resasco, Carbon 39 (2001) 547.

[30] A.M. Rao, E. Richter, S. Bandow, B. Chase, P.C. Eklund, K.A. Williams, S. Fang, K.R. Subbaswamy, M. Menon, A. Thess, R.E. Smalley, G. Dresselhaus, M.S. Dresselhaus, Science 275 (1997) 187.